Jurnal Teknik Sipil & Perencanaan 26 (1) (2024) p 17 - 29

JURNAL TEKNIK SIPIL & PERENCANAAN

10.15294/jtsp.v26i1.48630

Numerical Study of Steady Pipe Flows and Head Loss Coefficients

E.P. Bangun[1, a)] and N. Mahdi[1]

[1]Department of Civil Engineering, Universitas Sumatera Utara
Jl. Almamater, Padang Bulan, Medan 20155, Sumatera Utara, Indonesia

[a)] Corresponding author: emma.patricia@usu.ac.id

Abstract. The study concerns steady pipe flows within 90°-bend and T-junctions, the head loss coefficients, and the physical mechanisms responsible for the energy loss. Numerical viscous flow modeling based on SimpleFOAM solver was implemented in the study. Although secondary flow acts as the mechanism of energy loss in both the bend and the branch flow of the T-junction, the head loss coefficient in the former more critically depends on the Reynolds (*Re*) number. This is supported by the comparison of the streamlined fields and the radially varying profiles of the pressures from both cases. The location of flow separation prior to the secondary flow in the bend changes with *the Re* number, unlike the fixed location at the junction in the branch flow. The study confirms a practical implication related to the dependence of the head loss coefficients for pipes with 90°-bend and T-junction on flow velocity in a pipe network analysis.

Keywords: Steady pipe, Head loss, Numerical Study

INTRODUCTION

A pipe network is essential to daily human lives because it provides clean water and gasses for daily home and industrial activities. With the increasing number of human populations worldwide, underground pipe networks have become more complex. The network typically requires the installation of pipe junctions and bends to direct the flow to the consumers' destination and valves to dictate the flow discharge. Ensuring that the pressure and velocities have values lower than their safe maximum and achieve their required values is utterly essential. As a result, pressure and head loss associated with friction, valves, pipe junctions, and bends must be accurately predicted when designing a pipe network.

Commercial and open-source software has been employed by many designers to model and predict a pipe network. Such software typically assumes independence of head loss coefficients associated with friction on flow parameters. This may be acceptable when the flow is fully developed and the Reynolds (*Re*) number is huge; the latter is applied for a *Re* number larger than 10^8 in the case of a smooth pipe [1]. However, flow discharge and pipe diameters utilized for water consumption may be set such that the *Re* number is much lower than 10^8. Furthermore, flow separation may occur and disrupt a fully developed pipe flow that enters a bend or a junction. It is well known that flow separation around a circular cylinder is generally influenced by *Re* number [2, 3]. Nevertheless, the head loss coefficients for a pipe bend and junction are commonly treated as independent constants of *Re* number [4, 5]. As a result, evaluating the potential dependence of these minor head loss coefficients is essential.

The present study aims to investigate the head loss coefficients for cylindrical pipe numerically flows within bends and T-junctions and physically understand the mechanisms that cause their dependency on *the Re* number. Few

studies have employed computational fluid dynamics to evaluate this topic [6]. In this study, SimpleFOAM, a viscous flow solver for steady flows available in OpenFOAM (Version 2.3.0) [7], was utilized to model three-dimensional steady pipe numerical flows within the two geometries. This modeling is the most appropriate for pipes with circular cross-sections. Notably, the numerical model provides access to a wealth of data that helps a researcher understand the underlying physics. Since three-dimensional modeling is computationally costly, this study considers bend or T-junction within a pipe segment bounded by an inlet and outlet.

Test Cases

In the present study, pipes with 90^o-bends and T-junctions are considered. Table 1 presents the dimensions of the two types of pipes. These dimensions were determined from the pipe network data that serves the PDAM Tirtanadi consumers in the Sei Agul District of Medan, Indonesia and are presented in [8]. Given the radius of the pipe, r_p, relative to the radius of bend, $_{bend}$, the case of 90^o-bend is classified as a curved pipe [6].

TABLE 1. Cases and pipe dimensions are considered in the present study.

Case 1	Pipe with 90^o-bend	The radius of the pipe, r_p = 0.045 m	Radius of bend, r_{bend} = 0.5 m
Case 2	Pipe with T-junction	The radius of the pipe, r_p = 0.045m	

RESULTS AND DISCUSSION

Convergence Study of Pipe Flow Within the 90^o-Bend

The first numerical viscous flow modeling aims to investigate the head loss coefficients for the steady flows within the pipe with the 90^o-bend. Three types of boundary surfaces, namely wall, inlet, and outlet, enclose the computational fluid domain within the pipe. The fluid flow enters the domain through the inlet and exits the domain through the outlet. The three boundary conditions for all the boundary surfaces were set as follows. The boundary surface attached to the wall was defined as a **no-slip** boundary condition. The pressure variable on this surface had a **zero gradient** boundary condition. On the inlet of the fluid domain, the velocity was set to nonzero while the pressure was to be predicted. As a result, **FixedValue** was chosen for the boundary condition of the velocity variable, and **ZeroGradient** was set as the boundary condition of the pressure variable. For the outlet, the vice versa was applied to achieve numerical stability. In other words, **ZeroGradient** and **FixedValue** were thus chosen as the boundary conditions for the velocity and the pressure variables on the outlet, respectively.

Before running a numerical simulation, a pre-processing that generates mesh must be undertaken. The study employed *SALOME*, an open-source mesh-generating software. The first step of the pre-processing in this software was to define a divided disk, also known as a primary object. In order to set up the pipe with the 90^o-bend, five blocks were defined, while the pipe radius, r_p, was prescribed. The following step was to make points and a connecting line that formed the pipe. This stage helped create the pipe bend by choosing an option of *the fillet*. In this stage, the pipe bend radius, r_{bend}, had to be defined. Finally, the complete pipe geometry with the 90^o-bend was created by calling the *extrusion along the path* command. For this final stage, the pipe length was prescribed in any direction. An *x-y* plan view of the complete pipe geometry with the 90^o-bend and the locations of the inlet and outlet are presented in Fig. 1. Having created the pipe geometry, a structured mesh consisting of a finite number of hexahedral cells was generated. This mesh is considered to have better accuracy than an unstructured mesh [9, 10].

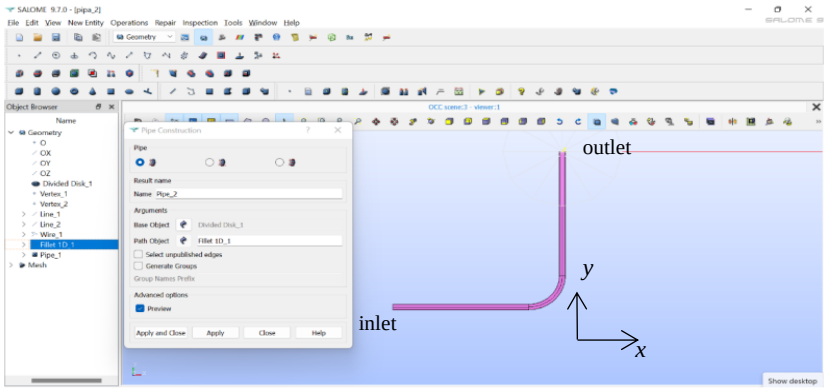

FIGURE 1. An *x*-*y* plane view of the complete pipe geometry with the 90º-bend.

In the case of pipe with the bend, the fluid velocity on the inlet, u_{inl}, was set to 0.12 m/s. This was estimated by undertaking an EPANET simulation of the pipe network that serves the PDAM Tirtanadi consumers in the Sei Agul District of Medan, North Sumatra, Indonesia [8]. In this case, the radius of the pipe, r_p, and the radius of bend, r_{bend}, correspond to Case 1 outlined earlier in Table 1. In respect of the pressure acting on the outlet, the value was set to zero. The pressure predicted on the inlet thus physically means the pressure drop or pressure difference that arises when the water flows from the inlet to the outlet. In the present study, the pressure drop, ΔP, is the average of the pressures computed on all surfaces of the numerical cells adjacent to the inlet. Furthermore, the pipe length in x and y directions, l_x and l_y, were both set to 5 m; this being approximately equal to 55D, where D the diameter of pipe. The choice of dimension follows the suggestion given in [6] and [11] to ensure that the inlet and outlet boundaries were sufficiently far enough not to be disturbed by local pressure changes due to the bend.

In undertaking a convergence study for this steady flow, various levels of mesh densities were considered. The level of mesh density depends on the radial size of the cell, D_r, defined as D/N_r, with N_r being the number of cells across the diameter of the pipe. Four levels of mesh densities were implemented, referred to as very coarse, coarse, medium, and fine mesh. For each level of mesh density, the N_r value, the number of cells generated in the computational domain, N_{cell}, the computational time required to run a simulation, $_{Tsim}$, the pressure drop, ΔP, and the percentage of difference, PD, are presented in Table 2. Figure 2 shows the cross-sectional views of the numerical cells generated under the various levels of mesh densities. It shows that the fine mesh has the most refined cells. Furthermore, the PD value herein quantitatively indicates the discrepancy between the pressure drops, ΔP, generated in one case of level of mesh density and the case of fine mesh. Each numerical simulation was run on a personal computer with an Intel(R) Core (TM) i5-8265U CPU processor @ 1.60GHz 1.80 GHz.

TABLE 2. Comparisons of Radial Size of Cell, Number of Cells, Computational Time, Pressure Drop, and Percentage of Difference Generated in Varying Cases of Levels of Mesh Densities.

Level of Mesh Density	Radial Size of Cell, D_r	Number of Cells, N_{cell}	Computational time, $_{Tsim}$ [min]	Pressure Drop, ΔP [Pa]	Percentage of Difference, PD [%]
Very Coarse	D/6	1200	1.0	1.79	77.00
Coarse	D/12	9600	3.0	4.70	40.00
Medium	D/24	76800	12.0	7.30	6.43
Fine	D/48	614400	42.0	7.80	0.00

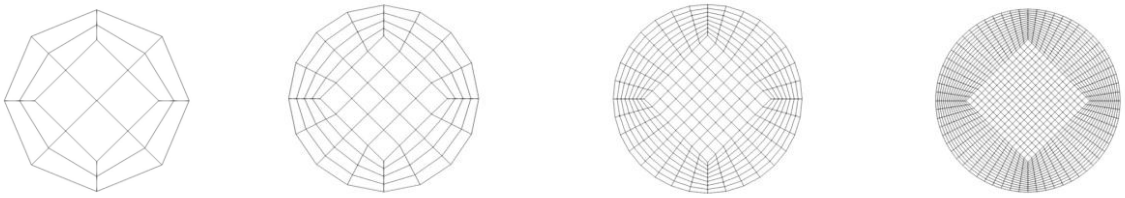

(a) (b) (c) (d)

FIGURE 2. Cross-sectional views of the numerical cells generated under different levels of mesh densities: (a) very coarse mesh, (b) coarse mesh, (c) medium mesh, and (d) fine mesh.

Based on the data in Table 2, two critical points can be deduced herein. First, the computational time, t_{sim}, increases with the N_r value and N_{cell} value. Second, the percentage of difference, *PD*, indicates the convergence of the present numerical simulations. Indeed, Fig. 3(a) confirms that the pressure drop, ΔP, computed using the various levels of mesh densities, converges to 7.80 Pa. To further confirm the convergence, the head loss coefficient, *k*, was computed for each level by using this modified Bernoulli equation.

$$k = \left(\frac{\Delta P}{\rho g} + \frac{u_{inl}^2 - u_{out}^2}{2g}\right)\frac{2g}{u_{inl}^2} \quad (1)$$

P_{inl} and P_{out}, respectively, denote the averaged pressures acting on the inlet and outlet. The difference between these two defines the pressure drop, ΔP—similarly, u_{inl} and u_{out} express the averaged water velocity at the inlet and the outlet. In the present model, the elevations of these two boundaries are equal. Following [11], the averaging was undertaken by implementing a surface integration on each variable's inlet and outlet. Figure 3(b) shows the head loss coefficient, *k*, for each level of mesh density. The coefficients converge as the number of cells increases. Given the short computational time for the case of medium mesh and its small percentage of difference (see again Table 2), the medium mesh is considered optimal for predicting the head loss coefficient accurately.

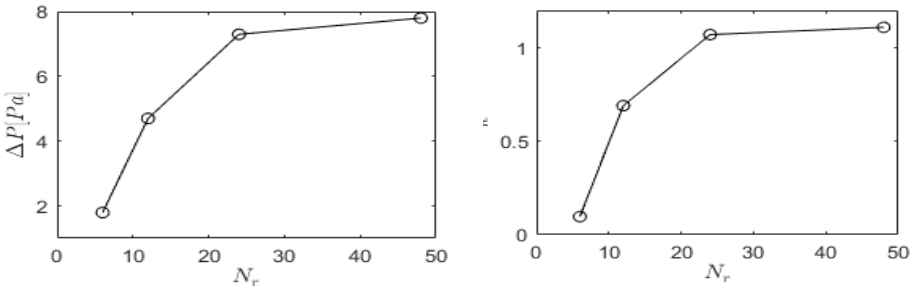

(a) (b)

FIGURE 3. Variations of (a) the pressure drop, ΔP, and (b) the head loss coefficient, *k*, with level of mesh density.

The head loss coefficient, *k*, predicted from the present numerical study for the bend case (i.e. k=1.198, see again Fig. 3(b)), lies in the range of coefficient values experimentally measured by [4] (i.e. 0.3 <=k<=1.5). The lowest *k* value in the range was observed in the case of flanged bend with long radius, while the highest one was proven from the opposite cases. The *k* value obtained from the numerical simulation is comparable to the experimental data. Given this comparison, the present numerical model of the steady flow within the pipe bend using the SimpleFOAM is validated. It should be noted, however, that the comparison is satisfactory. This is at least due to the negligible wall roughness considered in the numerical modeling and the potential dependence of *the k* value on the fluid velocity (or *Re* number).

Convergence Study of Pipe Flow Within a T-junction

In this case, the T-junction has one inlet and two outlets. The types of boundary conditions for walls and for inlet and outlet defined in the earlier case were again implemented in the present numerical model. In making the geometry, *SALOME* was again employed, and *T Shape Fluid* was chosen as the primary object. For this stage, the radius of the pipe and the pipe length in any direction were prescribed. Figure 4 shows an *x*-*y* plane view of the complete geometry of the pipe with a T-junction. This figure shows that the pipe with a T-junction has one inlet and two outlets; the first and second outlets are referred to as outlet1 and outlet2, respectively. Whether a boundary surface acted as an inlet or outlet was also determined from the EPANET simulation conducted earlier [8].

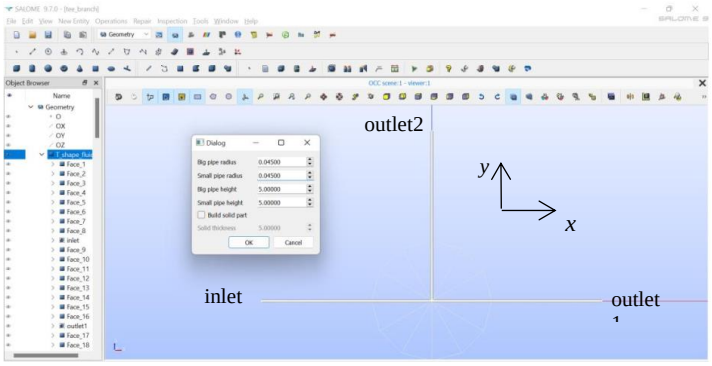

FIGURE 4. An *x*-*y* plane view of the complete pipe geometry with a T-junction

The velocity at the inlet, u_{inl}, was estimated to be 0.27 m/s. In this case, the pipe radius, r_p, corresponds to Case 2, outlined earlier in Table 1. Given all the data, the corresponding *Re* number was thus 24300. Having set up the boundary conditions for all boundary surfaces, the flow domain was solved again using the SimpleFOAM viscous flow solver. In the setup, the pipe length in any direction was chosen so that the inlet and outlet were sufficiently far enough not to be disturbed by local pressure changes in the T-junction.

A convergence study involving various levels of mesh densities was also conducted. Table 3 provides the values of D_r, N_{cell}, t_{sim}, ΔP, and *PD* for five different levels of mesh density. With the increasing mesh density and decreasing *PD* value, Table 3 indicates the convergence of the result.

TABLE 3. Comparisons of Radial Size of Cell, Number of Cells, Computational Time, Pressure Drop, and Percentage of Difference Generated in Various Levels of Mesh Densities

Level of Mesh Density	Radial Size of Cell, D_r	Number of Cells, N_{cell}	Computational time, t_{sim} [min]	Pressure Drop, ΔP [Pa]	Percentage of Difference, *PD* [%]
Very Coarse	*D*/8	256	0.5	14.20	64.00
Coarse	*D*/12	864	2.0	16.30	57.20
Medium	*D*/24	6912	6.0	27.10	27.90
Fine	*D*/48	55296	24.0	34.70	7.44
Very Fine	D/96	442368	52.0	37.50	0.00

To further evaluate the convergence, the variations of the head loss coefficients arising when the fluid flows into outlet1, k_1, and outlet2, k_2, are evaluated from these modified Bernoulli equations:

$$k_1 = \left(\frac{\Delta P}{\rho g} + \frac{u_{inl}^2 - u_{out1}^2}{2g}\right)\frac{2g}{V_{inlet}^2}, \tag{2}$$

$$k_1 = \left(\frac{\Delta P}{\rho g} + \frac{u_{inl}^2 - u_{out1}^2}{2g}\right)\frac{2g}{u_{inl}^2}, \tag{3}$$

where u_{inl}, u_{out1} and u_{out2} are the averaged velocities at the inlet, outlet1 and outlet2, respectively. Figure 5(a) shows the variation of the pressure drop with the level of mesh density, while Figs. 5(b) and (c) present the corresponding variations of the head loss coefficients arising when the fluid flows into outlet1, k_1, and outlet2, k_2, respectively. These figures confirm that the present simulations have reached converged results with the increasing N_r value. For the fine mesh, the number of cells, N_{cell}, was 55296, and the required computational time was 24 minutes.

Furthermore, the value of ΔP is estimated to be 34.70 Pa, while the k_1 and k_2 values are found to be 1.21 and 1.95, respectively. Gerhart et al. [4] previously measured the head loss coefficient for a pipe with a T-junction. This measured coefficient varies in the range of $0.2<k<0.9$ for a line flow and $1.0<k<2.0$ for a branch flow. The coefficient's exact value depends on the pipes' connection type. Herein, a line flow refers to the flow going into the first outlet (outlet1),

and a branch flow corresponds to the flow entering the second outlet (outlet2). Given the range measured from the earlier laboratory study, the head loss coefficient predicted in the present study is considered reasonable. Figures 5(b) and (c)) also confirm that the head loss coefficient for the line flow (outlet1), k_1, is smaller than that for the branch flow (outlet2), k_2. This is also in agreement with the earlier study. Moreover, the velocities at the first and second outlet, u_{out1} and u_{out2}, were predicted to be 0.231 m/s and 0.048 m/s, respectively. These two predictions indicate that the law of mass continuity has been satisfied.

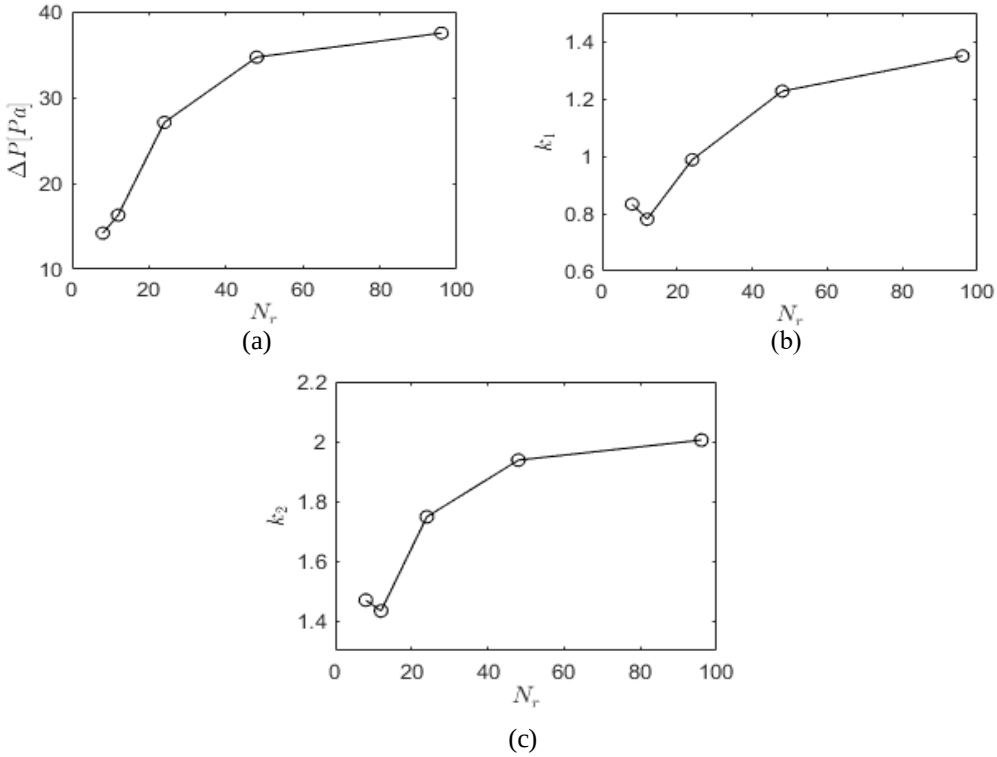

FIGURE 5. (a) The pressure drops, ΔP, and (b) the head loss coefficients arise when the fluid flows into outlet1, k_1, and (c) outlet2, k_2 over various levels of mesh density.

Comparison of Fluid Flows

Figure 6(a) presents the field of velocity magnitude, u_{mag}, that exists within the bend, while Fig. 6(b) shows the field of u_{mag} within the T-junction, with its close-up view provided in Fig. 6(c). The velocity magnitude, $\underline{u}_{\text{mag}}$, is indicated from the legend, while the arrows on the streamlines present the flow direction. The velocity near the outer wall of the bend has larger magnitude. This is similar to the findings in [9], [12] and [13]. In both bend and T-junction cases, flow separations occur. This mainly generates multiple vortices when the water passes through the T-junction (see Figs. 6(b) and (c)). Interestingly, a secondary flow exists when the flow direction has to change. This is confirmed from both the bend case, in which the flow direction changes gradually (Fig. 6(a)), and the T-junction case, in which an abrupt change of flow direction occurs in the branch flow (Fig. 6(b)).

The secondary flow in the bend occurs following a flow separation near the bend entrance and inner wall. Interestingly, in the case of T-junction, the secondary flow only occurs in the branch flow and begins at the junction. The branch flow differs from the line flow. This is consistent with the head loss coefficient associated with the outlet2, k_2, which has an unidentical value to that corresponding to the outlet1, k_1 (see Figs. 5(b) and (c)). The k_2 coefficient is greater than the counterpart. This comparison and the flow visualizations within the T-junction indicate that the energy loss arising in the branch flow is more significant than in the line flow.

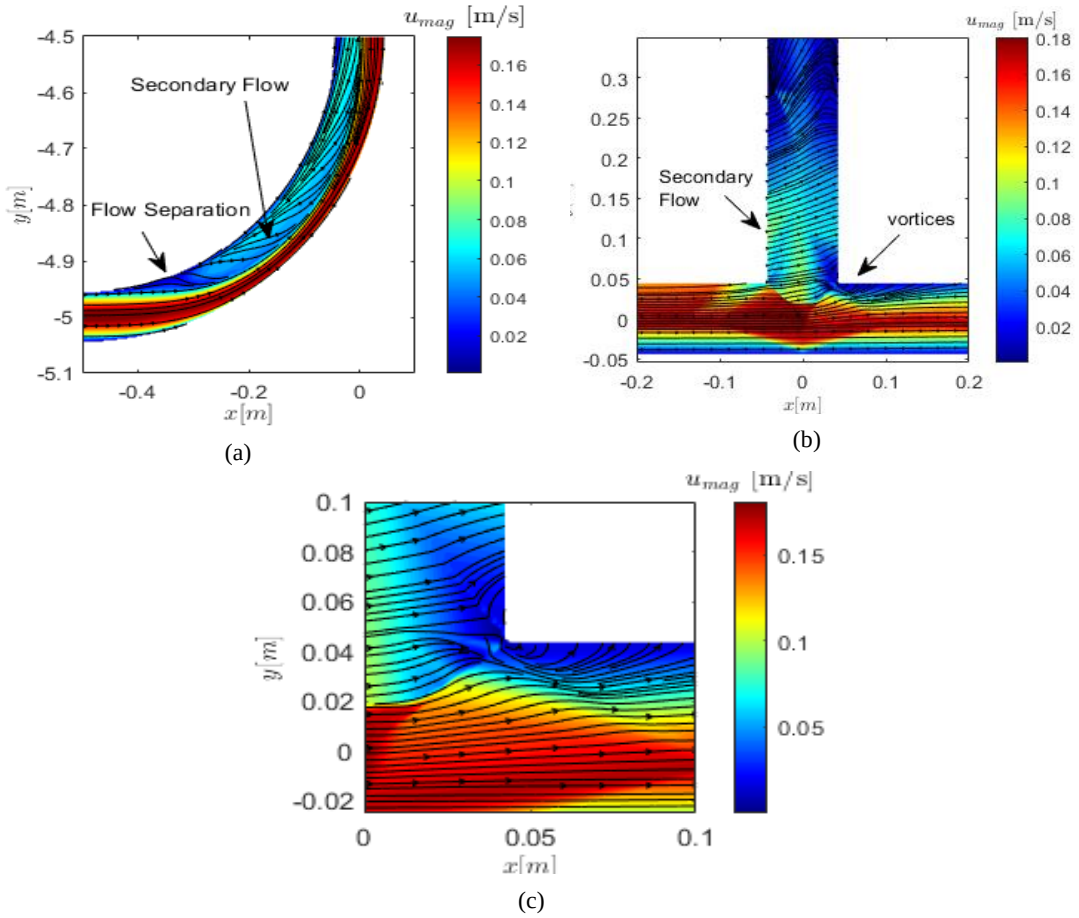

FIGURE 6. Field of velocity magnitude, u_{mag}, and streamlines of the flow within the pipe near (a) the bend and (b) the T-junction with (c) its close-up view.

Effects of Reynolds Number

Pipe Flows Within Bends

The head loss coefficients for the pipe with bend over varying *Re* number are investigated. The aim of this investigation is to confirm any dependence of the coefficient on the *Re* number. The *Re* number was varied by changing the velocity at the inlet (or inlet velocity), u_{inl}. This velocity was determined using EPANET simulations that considered the fluctuation of water consumption in one day. The time-varying discharge of water refers to the data of water-consumption percentage issued by the General Directorate Cipta Karya Air Bersih [14].

Various *Re* numbers considered herein lie in the range of $7200 \leq Re \leq 20700$ in the cases of pipe with bend. By implementing Equation (1), the head loss coefficient, *k*, was predicted. The variation of the head loss coefficient with the *Re* number is presented on Fig. 7(a). It shows that the head loss coefficient significantly decreases with the *Re* number. Increasing almost three times the *Re* number reduces the *k* value by half of the initial *k* value (i.e., $k = 2.11$). This is unexpected given that the head loss coefficient for the flow within a pipe with a bend is traditionally believed to be independent of *the Re* number [4, 5]. There might have been the contribution of wall friction (or significant loss) along the pipe length before and after the bend to this dependence. The head loss coefficient was re-computed to verify this potential by considering a new inlet and an existing outlet in the present numerical simulations. The former was chosen at a cross-section where the location was very close to the bend, and the secondary flow had not occurred. Thecated at the belocatedentrance, while the new outlet was set to the exit. By computing the averaged velocities and the averaged pressures at these two cross-sectional areas and implementing Equation (1) again, the head loss

coefficient associated with the bend, k_{bend}, was estimated. The variation of k_{bend} with the *Re* number is presented in Fig. 7(b). It shows that the k_{bend} value indeed varies with the *Re* number. Increasing almost three times the *Re* number reduces the k_{bend} value by more than 60% of the initial k_{bend} value (i.e. k_{bend} = 0.49). This indicates that the energy loss arising in the bend due to the change in flow direction is not a function of the square of the fluid velocity. It is a higher-order function of the velocity. Ito's formulae [15] predict that the $_{bend}$ is 0.36 when *the Re* number is 10500, and the ratio of $_{bend}/r_p$ is 11.11. This k_{bend} value is very close to the present prediction (see Fig. 7(b)).

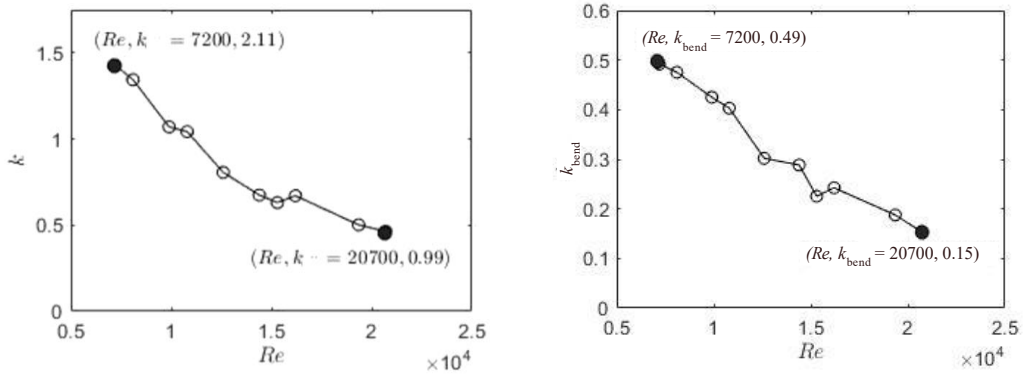

(a) (b)

FIGURE 7. Variation of (a) the head loss coefficient, k, and (b) the head loss coefficient associated with the bend, k_{bend}, with *Re* number in the case of pipe with a 90°-bend.

In order to further confirm the dependence of the *Re* number, the radially varying profiles of velocity and pressure on an *x*-*y* plane with z = 0 m require an investigation. The velocity magnitudes, u_{mag}, and the pressures, p, across the radius of the pipe relative to its diameter, r/D, at certain locations, l', relative to the length of the bend, l_{bend}, are presented. Herein, l_{bend} is defined as the perimeter of the bend and quantified as $0.5\pi r_{bend}$, with r_{bend} being the radius of bend. Figures 8(a)-(d) show the radially varying profiles of the velocity magnitudes, u_{mag}, normalised by the corresponding inlet velocities, u_{inl}, respectively at $l' = 0.25l_{bend}$, $l' = 0.50l_{bend}$, $l' = 0.75l_{bend}$ and $l' = 1.0l_{bend}$ for three different *Re* numbers of 7200, 14400 and 20700. The positive r/D values in Fig. 8 indicate the radial locations near the inner wall, while the negative r/D values are closer to the outer wall. The velocity profile at $l' = 0.75l_{bend}$ near the inner wall (positive r/D values), where the secondary flow occurs, appears to vary with the *Re* number (see Fig. 8(c)). Overall, the velocity profiles at various locations slightly vary with the *Re* number.

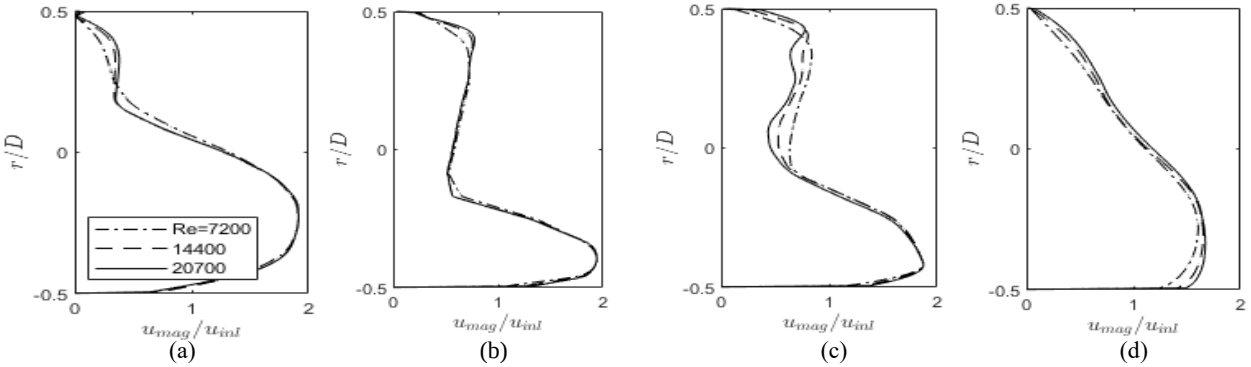

(a) (b) (c) (d)

FIGURE 8. Radially varying profiles of the velocity magnitudes, u_{mag}, normalized by the corresponding inlet velocities, u_{inl}, at locations of bend: (a) $l' = 0.25l_{bend}$, (b) $l' = 0.50l_{bend}$, (c) $l' = 0.75l_{bend}$ and (d) $l' = 1.0l_{bend}$ for *Re* numbers of 7200, 14400 and 20700.

The slight variation of the velocity profile with the *Re* number contrasts with the variations of the pressure profile. Figure 9 confirms the significant variation of the pressure profile with the *Re* number; herein, the pressure, p, is

normalized to the square of the velocity at the inlet, u^2_{inl}. The importance of *Re* number is most evident at lower range of *Re* numbers (i.e. 7200 ≤ *Re* ≤ 14400) and becomes less pronounced with the increasing *Re* number (i.e. 14400 ≤ Re ≤ 20700). This suggests the negligible variation of head loss coefficient at huge *Re* numbers. Nevertheless, this study confirms important practical implications because the present range of *Re* numbers is chosen from the actual data of an existing pipe network. As such, predicting pressure at the nodes of a pipe network involving pipes with 90°-bends should consider the dependence of the head loss coefficient on *Re* number. This contradicts the common practice in an analysis of pipe flow that assumes a fixed head loss coefficient regardless of the flow discharge.

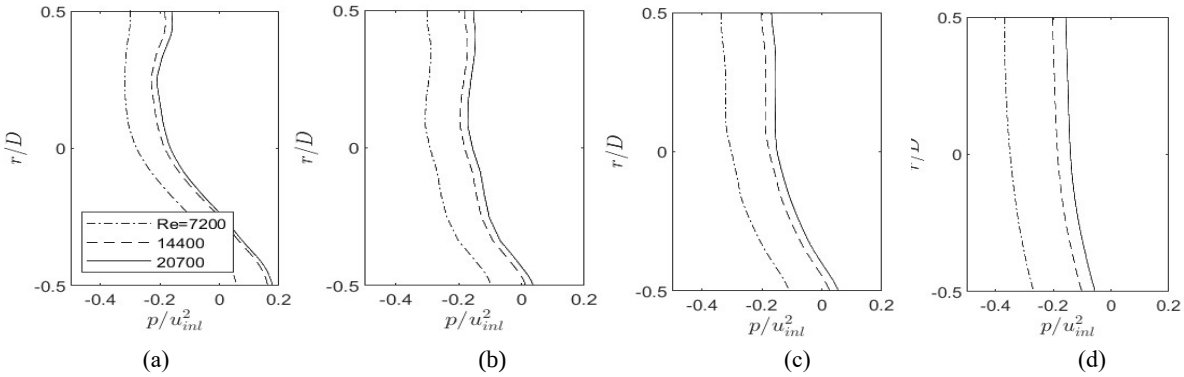

FIGURE 9. Radially varying profiles of normalized pressures, p/u^2_{inl}, at certain locations of bend: (a) $l' = 0.25l_{bend}$, (b) $l' = 0.50l_{bend}$, (c) $l' = 0.75l_{bend}$ and (d) $l' = 1.0l_{bend}$ for three different *Re* numbers of 7200, 14400 and 20700.

The fields of velocity magnitude, u_{mag}, at the *Re* numbers of 7200 and 20700 are presented on Figure 10. It shows that with the increasing *Re* number, the location of flow separation moves further upstream, changing the extent of the secondary flow. This is consistent with the results presented in [9]. Notably, the field further confirms the dependence of the head loss coefficient for pipe with a 90°-bend on the *Re* number.

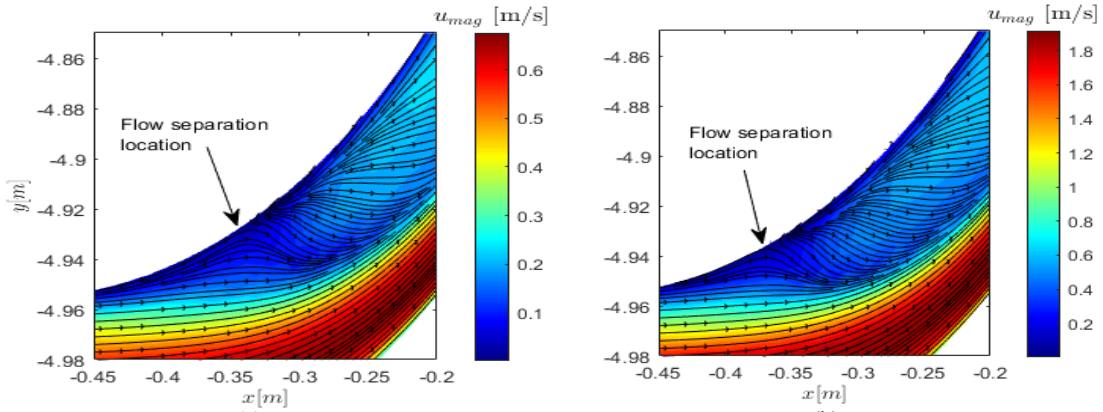

FIGURE 10. Velocity fields and streamlines of the flows within the pipe near the bend at *Re* numbers (a) 7200 and (b) 20700.

Pipe Flows Within T-junction

The effect of the *Re* number on the flow within the pipe with T-junction is also investigated. Similarly, the velocity at the inlet varied while the pipe diameter, pipeand wa, andmeters were kept constant. The variation of the inlet velocity was again determined using the data of water-consumption percentage issued by the Public Work Service of the General Directorate Cipta Karya Air Bersih [14]. As a result, the *Re* numbers considered vary in the range of 6300 ≤ *Re* ≤ 24300.

Figure 11 presents the variations of the head loss coefficients associated with outlet1 and outlet2, k_1 and k_2, with the *Re* number in the cases of pipes with T-junction. Again, outlet1 corresponds to the line flow, and outlet2 is the

branch flow. It shows that both the k_1 and k_2 values decrease less than 50% of its initial values when the *Re* number increases fourfold. This reduction in the k_1 and k_2 values is less significant than that in the cases of pipes with bend. Nevertheless, the dependence on the *Re* number is considered necessary since the decrease is more than 40% of the initial k_1 value and 20% of the k_2 value at Re=6300; the head loss coefficient associated with the outlet1 (line flow) being more critically dependent on *Re* number. This dependence is also unexpected given that many literature studies confirm the independence of the head loss coefficient for pipes with T-junction on *Re* number [4].

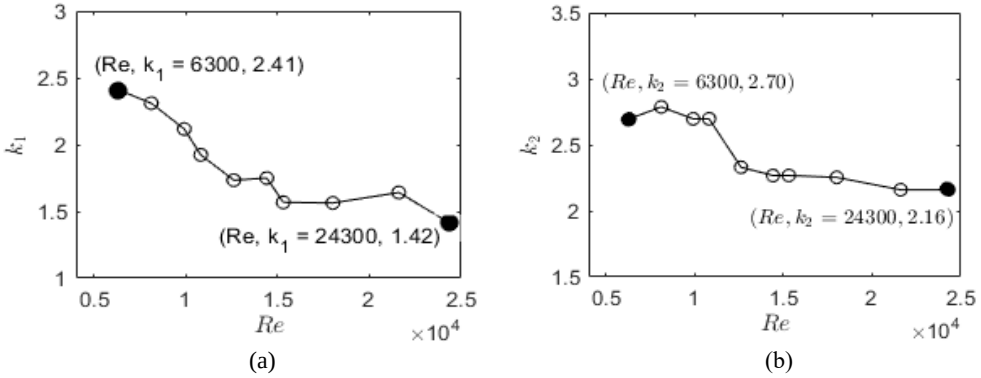

(a) (b)

FIGURE 11. Variation of the head loss coefficient associated with (a) outlet1, k_1, and (b) outlet2, k_2, with *Re* number in the case of T-junction with one line flow and one branch flow.

To further confirm the dependence of the k_1 and k_2 values on the *Re* number, the radially varying profiles of velocities and pressures on an *x*-*y* plane with $z = 0$ m at locations near the T-junction are investigated. Three different *Re* numbers are considered fixed at 6300, 12600, and 21600. Figure 12(a) presents the radially varying profile of velocity at the location prior to the T-junction when $x = -0.2$ m, while Figs. 12(b) and (c) respectively show the velocity profiles of u_{mag}/u_{inl} at two different locations after the T-junction; one within the line pipe and the other within the branch pipe. The location of the former was set to $x = 0.2$ m, while the latter was prescribed at $z = 0.2$ m. The velocity profiles computed at $x = -0.2$ m and 0.2 m slightly vary with the *Re* number more than within the branch flow. However, the velocity magnitude within the branch flow is relatively small. Therefore, the influence of changes in this velocity profile on the variation of the k_2 values with the *Re* number is considered insignificant.

Fig. 13 presents the corresponding variations of pressure profiles of p/u^2_{inl} with *Re* number. Figure 13(a) shows the profiles at the location before the T-junction, while Figs. 13(b) and (c) describe those at the locations after the T-junction within the line and branch flow, respectively. Figures 13(a)-(c) confirm that the pressure within the branch flow slightly depends on *Re* number. This is consistent with Fig. 11(b), which shows the less critical dependence of the k_2 coefficient on the *Re* number.

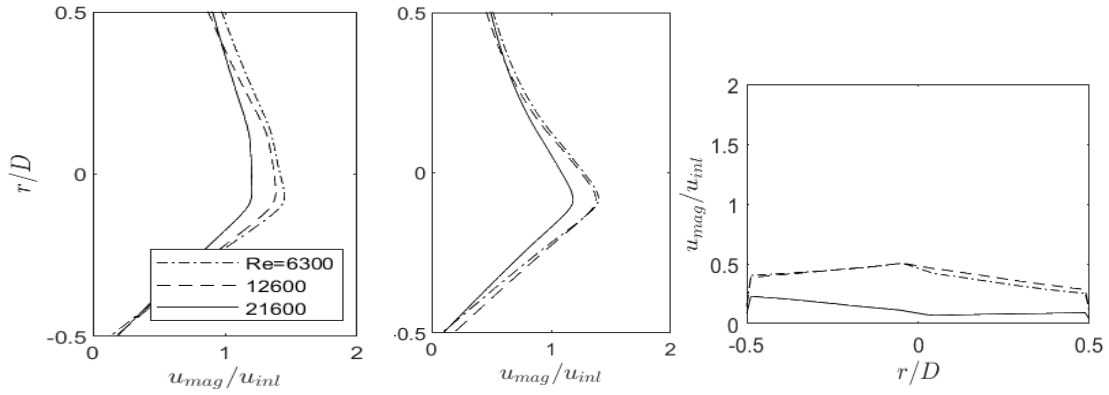

(a) (b) (c)

FIGURE 12. Radially varying profiles of normalised velocities, u_{mag}/u_{inl} at specific locations near the T-junction: (a) $x = -0.2$ m, (b) $x = 0.2$ m and (c) $z = 0.2$ m for three different *Re* numbers of 6300, 12600 and 21600.

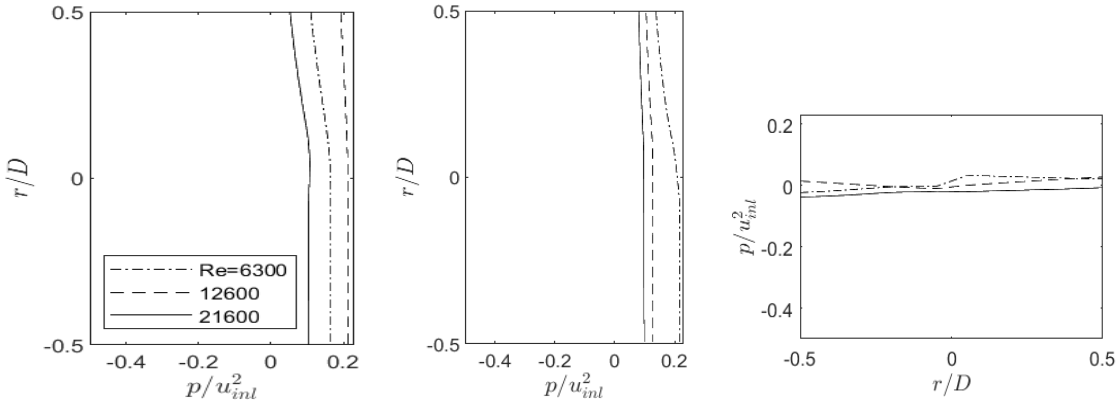

FIGURE 13. Radially varying profiles of normalized pressures, p/u^2_{inl}, near the T-junction at certain locations: (a) x = -0.2 m, (b) x = 0.2 m, and (c) z = 0.2 m for three different *Re* numbers of 6300, 12600 and 21600.

The fields of u_{mag} and the streamlines of the flows near the branch in the three cases of *Re* numbers further confirm the earlier finding. Figure 14 indicates that the vortex formation at the right corner of the branch varies with the *Re* number. As the inlet velocity increases, the vortex formation becomes less evident. In contrast, the secondary flows within the branch pipe appear to be similar regardless of the *Re* number. The secondary flow in the branch pipe always begins at the junction. This contrasts with the bend case (see Figs. 6(a) and 10). The secondary flow begins after the flow separates, and this separation's location depends on the *Re* number. The comparison indicates that the secondary flow is more predictable when the flow direction abruptly changes. This is analogous to the fixed location of flow separation when the flow separates from a corner or bluff body. Instead, when the flow encounters a streamlined body, the location of flow separation is more dependent on *the Re* number [3]. The more pronounced dependence of the head loss coefficient for the pipe with a bend than that in the branch flow thus has a physically grounded explanation. The energy loss in these two flows similarly occurs during a secondary flow. However, its starting location and the length over which the secondary flow exists may depend on the *Re* number.

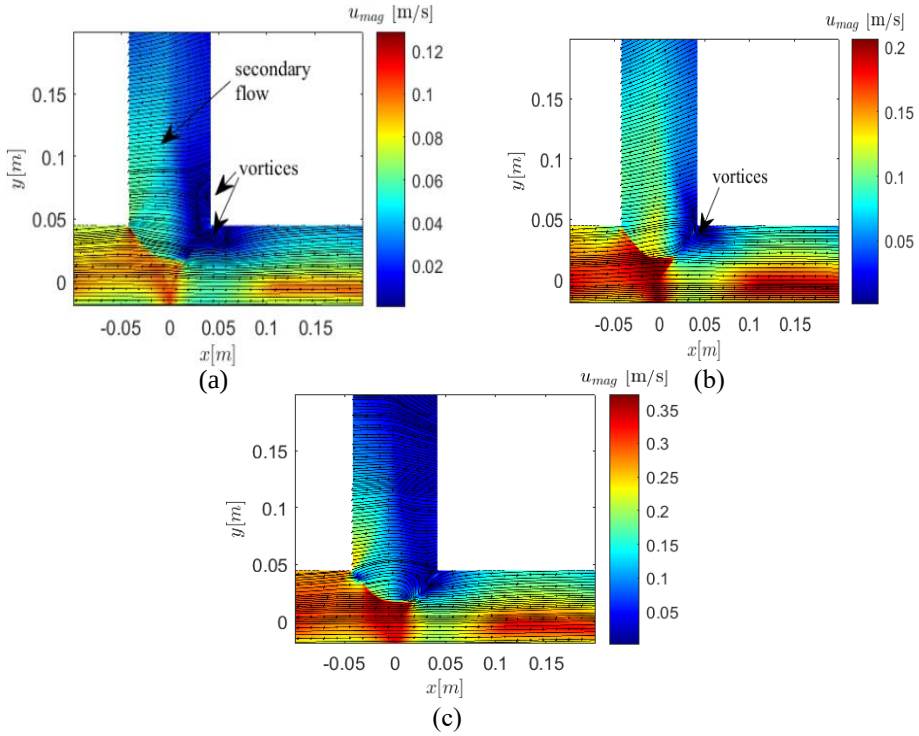

FIGURE 14. Field of velocity magnitude, u_{mag}, and streamlines of the flow near the T-junction at various *Re* numbers: (a) 6300, (b) 12600, and (c) 21600.

Following on, another case of T-junction with two branch flows is considered. The variations of the head loss coefficients, k_1, and k_2, with *Re* number, are presented in Figures 15(a) and (b). Both figures confirm that the k_1 and k_2 coefficients have equal values. This is unsurprising since the flow from the inlet separates symmetrically at the T-junction. Furthermore, Figure 15 confirms that the decreases of the k_1 and k_2 coefficients with the increasing *Re* numbers are approximately 30%, which is less significant than the percentage of decrease in the bent case (see again Figure 11(a)). Therefore, all the evaluations provided in the present study confirm that the dependence on the *Re* number for the flow within a pipe with a 90°-bend is more critical than in the case of a pipe with a T-junction.

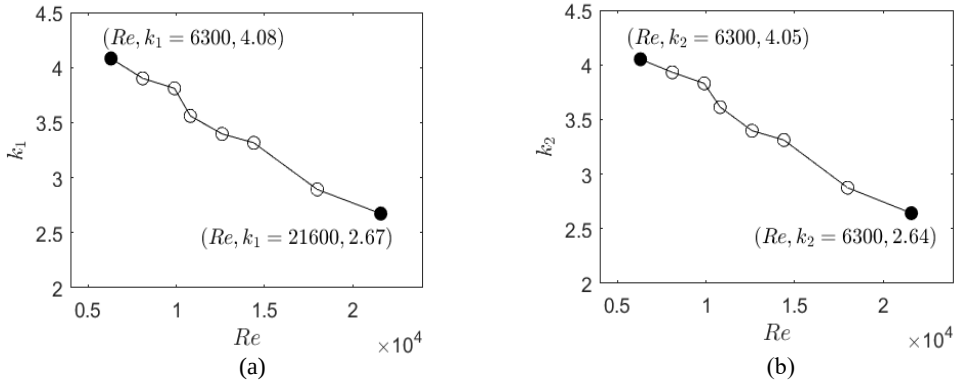

FIGURE 15. Variation of the head loss coefficient associated with (a) outlet1, k_1, and (b) outlet2, k_2, with *Re* number in the case of T-junction with two branch flows.

CONCLUSIONS

Steady pipe flows within bends and T-junctions were numerically modeled. Convergence studies were undertaken to determine the required grid arrangements to predict the head loss coefficients and pressure differences accurately. The mechanisms that cause the energy loss in the T-junction and the bend have been described. The former is associated with a secondary flow in the branch flow and vortices in the line flow. The latter is driven by a secondary flow following a flow separation at a specific location near the entrance of the bend.

The head loss coefficients in the bends and T-junctions were investigated. This indicates that these coefficients depend on the *Re* number. The radially varying profiles of pressures and the streamline fields evaluated over various *Re* numbers support this finding. The study thus recommends considering the variation in the coefficient with *the Re* number in an analysis of a pipe network that typically assumes constant head loss coefficients regardless of the flow velocity. Furthermore, the flow visualizations help explain why the bent case is more critically dependent on the *Re* number. The location where flow separates after the entrance of the bend depends on this number, changing the extent of the secondary flow. This significantly differs from the branch flow in which the secondary flow always begins at the junction.

REFERENCES

1. Moody, L. F., “Friction factors for pipe flow,” Transactions of the ASME 66 (1944).
2. Sarpkaya, T., “Forces on cylinders and spheres in a sinusoidally oscillating fluid,” Journal of Applied Mechanics 42 (1977).
3. Sarpkaya, T., “Forces on a circular cylinder in viscous oscillatory flow at low Keulegan-Carpenter numbers,” Journal of Fluid Mechanics 165 (1986).
4. Gerhart, P. M., Gerhart, A. L. and Hochstein, J. I., “Fundamentals of fluid mechanics,” (John Wiley & Sons, 2016).
5. Rossman, L., Woo., H., Tryby, M., Shang, F., Janke, R., and Haxton, T., "EPANET 2.2 User Manual, U.S. Environmental Protection Agency, Washington, DC (2020).
6. Crawford, N., “Pressure losses at bends and junctions”, Ph.D Thesis, Queen’s University Belfast (2005).
7. Greenshields, C., “Open foam: the open source CFD toolbox, version 2.4.0 edn, CFD Direct Ltd (2015).
8. Habibie, A. K., “Evaluasi jaringan perpipaan distribusi air bersih di kelurahan Sei Agul Kecamatan Medan Barat Kota Medan menggunakan aplikasi Epanet 2.2”, Laporan Tugas Akhir, Universitas Sumatera Utara (2022).

9. Dutta, P., Saha, S. K., Nandi, N. and Pal, N., “Numerical study on flow separation in 90^{o} pipe bend under high Reynolds number by k-ε modeling”, Engineering Science and Technology, an International Journal 19 (2016).
10. Yang, Z. Y., Savari, C. and Barigou, M., “Numerical and experimental investigations of horizontal turbulent particle-liquid pipe flow”, Industrial and Engineering Chemistry Research 61 (2022).
11. Vaszonyi, A., "Pressure loss in elbows and duct branches," Trans. American Society of Mechanical Engineers 66 (1944).
12. Weske, J. R., "Investigations of the flow in curved ducts at large Reynolds numbers," Journal of Applied Mechanics AIME 15 (1948).
13. Taylor, AMKP, Whitelaw, J.H. and Yianneskis, M., "Curved ducts with strong secondary motion: Velocity measurements of developing laminar and turbulent flow," Journal of Fluid Engineering 104 (1982).
14. General Directorate Cipta Karya Air Bersih, “Proyeksi Kebutuhan Air Dan Identifikasi Pola Fluktasi Pemakaian Air”, Kemenkeu PUPR (1996).
15. Ito, H., "Friction factors for turbulent flow in curved pipes," Journal of Basic Engineering American Society of Mechanical Engineers 81 (1959).